

## Reversible Manipulations of Room Temperature Mechanical and Quantum Transport Properties in Nanowire Junctions

Uzi Landman, W. D. Luedtke, Brian E. Salisbury, and Robert L. Whetten  
*School of Physics, Georgia Institute of Technology, Atlanta, Georgia 30332-0430*  
 (Received 1 March 1996)

The electrical conductance and principal structural and mechanical properties of gold nanowires, exhibiting reversibility in elongation-compression cycles at ambient conditions, were investigated using pin-plate experiments and molecular dynamics simulations. Underlying the reversible nature of the nanowires are their crystalline ordered structure and their atomistic structural transformation mechanisms, involving stages of stress accumulation and stress relief occurring through multiple-glide processes and characterized by a high critical yield stress value. [S0031-9007(96)00879-4]

PACS numbers: 73.40.Jn, 73.20.Dx, 85.Ux

Junctions are materials structures which form upon bringing bodies into proximal interaction, during the separation of contacting bodies, in the process of extension (e.g., pulling) of a material system, or in the course of growth (e.g., fabrication of thin film junctions). Past, as well as intensifying current, investigations of junctions have been motivated by the ubiquity of circumstances in which they may be formed; either naturally in the course of a physical process (as in the case of materials interfaces in relative motion with respect to each other where the frictional resistance to shear has been attributed [1] to the formation of interfacial junctions, or as the source of interfacial adhesive action) or intentionally (e.g., controlled generation of wires via the extension of materials contacts, as in the case of surface manipulations using tip-based methods [2–8], a break-junction technique [9], or by separation of wires in contact [10]). Moreover, recent theoretical predictions [2,11] and subsequent experimental observations [2–10] have revealed remarkable properties of such junctions, particularly three-dimensional nanometer scale wires, which are of fundamental as well as of potential technological interest in the areas of miniaturization and very large scale assembly and integration of electronic devices. These findings include the following: structural characteristics (i.e., crystallinity) [2]; mechanical response [2,5,7,8], characterized by ideal critical yield stress values, with elongation occurring through a sequence of plastic stress accumulation and relief stages associated with ordered and disordered atomic configuration of the wires, and portrayed in oscillatory behavior of the pulling force; electronic transport [3,4,6,8–10], exhibiting room temperature conductance quantization as well as possible transition to a localization regime in sufficiently long wires [4]; and predictions of magneto-transport effects [12], including magnetic switching and magnetic blockade [13], occurring through the shifting of electronic energy levels in nanowires by an applied longitudinal magnetic field.

In this paper we investigate experimentally and theoretically the ability to mechanically manipulate and

control the quantum conductance in gold nanowires at room temperature. In particular, we demonstrate, using pin-plate equipment and molecular dynamics simulations [1(b) and (c)], that variations in the quantum ballistic electronic transport in such wires are correlated with the nature of the mechanical response of the wires, and that such variations can be manipulated in a reversible manner in cycles of extension and compression of the wire. The trace in Fig. 1, obtained through the use of the experimental setup shown schematically in Fig. 2, displays the conductance of a wire (corresponding to a resistance variation spanning  $\sim 0.2$ – $1.0$  k $\Omega$ ), measured during an extension-compression cycle of the contact between a gold pin and a gold surface. The conductance of a nanowire which was allowed to extend until breaking (see inset to Fig. 1), exhibits a conductance staircase with step heights mostly of  $\sim g_0 = 2e^2/h$ , and occasionally of  $\sim 2g_0$ ,

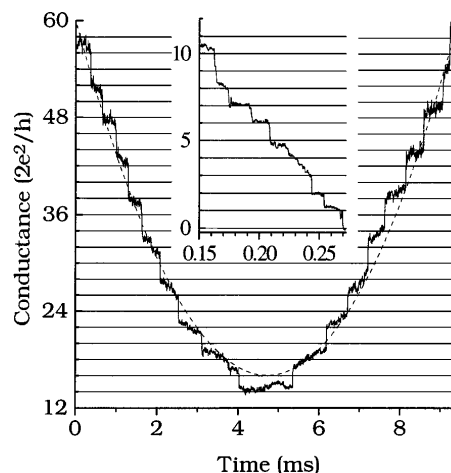


FIG. 1. Conductance, in units of  $2e^2/h$ , versus time, in ms, of a contact between a gold pin and a gold plate (see Fig. 2), measured at room temperature during an elongation-compression cycle. Displayed in the inset is a conductance trace recorded at the final stages of elongation of a wire which ultimately broke. A parabola (dashed line) is drawn to guide the eye.

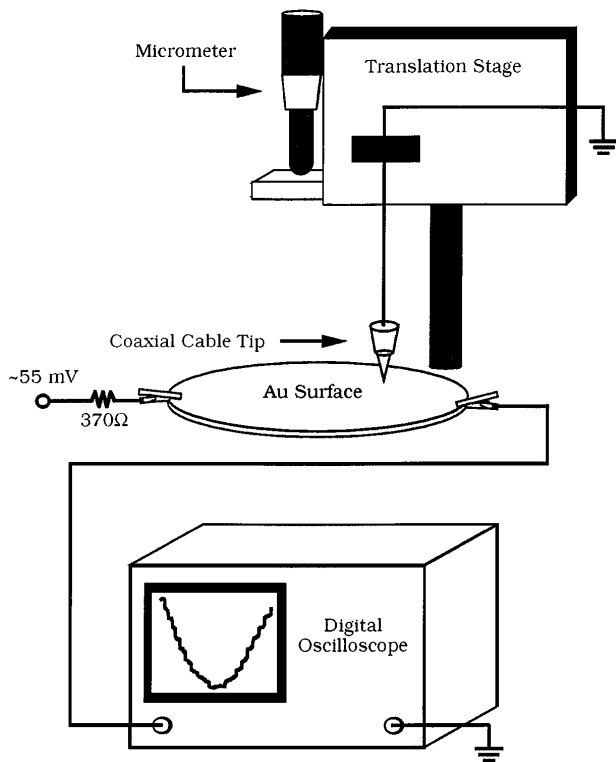


FIG. 2. Schematic of the pin-plate experiment. Electrical contact between a coaxial cable tip and the gold surface [Au on Cr on Si(111)] is controlled coarsely by a micrometer screw attached to an optical translation stage (the cable connecting to the tip is clamped to the translation stage). Nanometer scale tip displacements are likely caused by vibrations of the tip with respect to the surface. The digital oscilloscope (LeCroy 9304M) records the change in voltage across its internal resistance, caused by the change in current across the surface due to conduction through the nanowire to the grounded tip. The conductance is calculated from the data as  $G = (V_{\text{applied}}/V_{\text{measured}} - 1)/R_s$  where in our case the series resistance  $R_s = 370\Omega$  and  $V_{\text{applied}} = 55\text{ mV}$ .

corresponding to a small number of conducting channels in the ultimate stages of elongation of a wire and confirming room-temperature quantization of ballistic electronic transport through such wires. The conductance of the wire during the mechanical extension-compression cycle exhibits remarkable reversibility over 19 distinct plateaus, as well as uniformity in the time length of the plateaus and in the magnitudes of the step rises ( $\sim 4g_0$ , with a tendency toward smaller values when the nanowire is longer, i.e., closer to the middle of the cycle). Additionally, small slopes of the plateaus are observed, occurring in opposite senses about the middle of the cycle. It is of interest to remark that somewhat similar results were reported for much thicker Pb junctions at 4.2 K in ultra-high vacuum [5(b)], and under the same conditions for thicker Au junctions, using a combined scanning force and tunneling microscope [5(c)], showing shorter cycles and larger step rises (3 conductance steps, with step rises of the order of  $\sim 10g_0$ ), and were discussed in the con-

text of the results of earlier [2] molecular dynamics (MD) simulations.

Insights into the nature of the atomistic processes underlying the above observations are provided through large-scale MD simulations. In these simulations a crystalline gold wire oriented with the (111) direction parallel to the axis of the wire and containing 3273 atoms [1600 atoms treated dynamically and equilibrated initially as a 16-layer wire with the remaining atoms comprising Au(111) static substrates of 2 layers each, supporting the top and bottom of the wire] was modeled via the many-body embedded-atom potentials [14]. The wire was elongated by  $\sim 12\text{ \AA}$  [the spacing between adjacent (111) planes is  $2.35\text{ \AA}$ ] and subsequently compressed by the same amount at a rate of  $2\text{ m/s}$  ( $\sim 6 \times 10^{-4}$  of the longitudinal speed of sound in gold) under isothermal conditions at  $T = 300\text{ K}$ . Figure 3(a) depicts the pulling force (i.e., the force on the holder substrates at the top and bottom of the wire), and Fig. 3(b) shows the second invariant of the deviatoric stress tensor,  $J_2$ , which is proportional to the stored

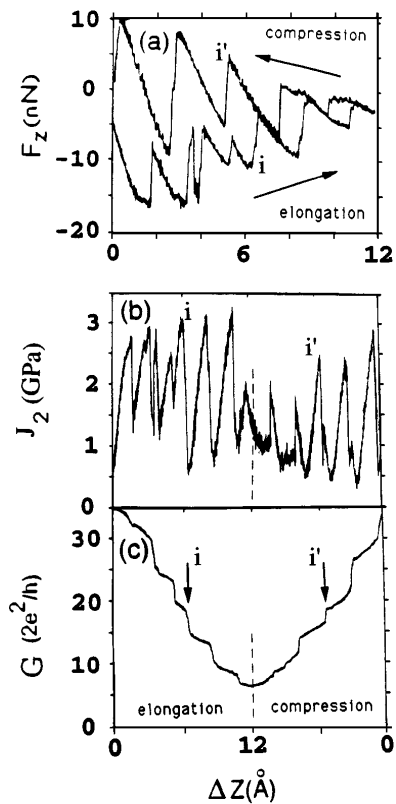


FIG. 3. Force [ $F_z$ , in nN, shown in (a)],  $J_2$  [in GPa, shown in (b)], and calculated conductance [ $G$ , in units of  $2e^2/h$ , shown in (c)], plotted versus displacement ( $\Delta z$ , in  $\text{\AA}$ ) obtained from MD simulations of elongation and compression of a (111) oriented gold nanowire at room temperature. In (a) the records for the elongation and compression stages are folded on the same distance scale, while in (b) and (c) they are plotted side by side with the reversal of the direction taking place at  $\Delta z = 12\text{ \AA}$ .

elastic energy available for shear deformation [2,15]. In Fig. 3(c) we display the conductance of the nanowire calculated from a semiclassical modification of Sharwin's expression [16]. Sideviews of atomic configurations with short-time trajectories recorded at selected stages during the elongation [4(a)–4(c)], and compression [4(a')–4(c')] are shown in Fig. 4.

Underlying the oscillatory sawtooth pattern of the forces in Fig. 3(a) and the corresponding behavior of  $J_2$  is the atomistic mechanism of the elongation and compression of the wire. These processes occur via a succession of alternating stress accumulation and relief stages (concentrating at a narrow section of the wire), during which the wire undergoes plastic structural transformations [2]. The nanowire's atomic structure is crystalline ordered in nature during most of the evolution of the wire [see, for example, Figs. 4(a), 4(c), 4(a'), and 4(c')]. However, this structure is strained during the stress accumulation stages, corresponding to the smaller slopes of the sawtooth patterns in Figs. 3(a) and 3(b). The ordered states of the wire are interrupted rather abruptly by brief transformation (yield) stages during which the wire is locally disordered. For wires as thick as those used in this study these transformations involve multiple glide processes primarily on (111)

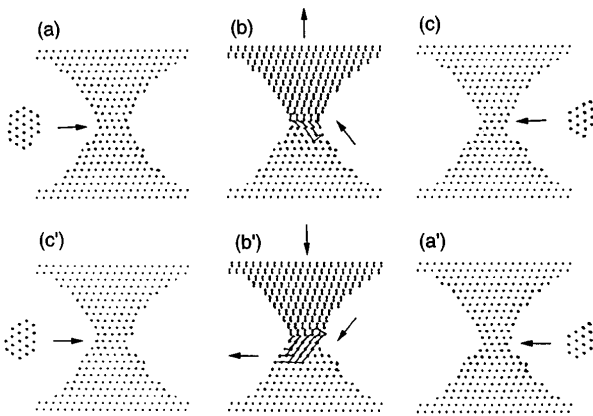


FIG. 4. Side views of atomic configurations (a), (c), (a'), and (c') and short-time trajectories (b) and (b'), in 5 Å thick vertical slices through the wire, recorded during the elongation (a)–(c) and compression (a')–(c') stages, marked  $i$  and  $i'$ , respectively. In Fig. 3, corresponding to transformation of the Au nanowire from 18 to 19 layers during pulling and the reverse during compression. Frames (a) and (c) and (a') and (c') correspond to before and after configurations, i.e., (a) and (c') correspond to a nanowire with 18 layers and (c) and (a') to 19 layers; included also are top cross-sectional views of the narrowest region of the wire. Frames (b) and (b') correspond to the fast structural transformation stages exhibiting multiple-glide processes (glide directions denoted by arrows); to indicate the atomic motions during the transformations, lines are drawn connecting the positions of atoms at the beginning and end of a 60 ps time interval. In each frame the two atomic layers at top and bottom correspond to the Au substrates supporting the wire.

planes [Figs. 4(b) and 4(b')], leading to elongation and narrowing [Figs. 4(a)–4(c)] or shortening and thickening [Figs. 4(a')–4(c')], of the nanowire. As seen from Fig. 3 [e.g., Fig. 3(a)], the mechanical and transport characteristic of the wire during elongation and compression are “phase shifted” with respect to each other. This effect, which has been observed experimentally [5], is due to the change from tensile to compressive stress upon reversal of the process from elongation to compression, respectively. Accompanying these processes are variations in the cross-sectional areas and shapes of the wire; note that the interaction of the glide planes with the periphery of the wire can cause areal and shape changes even in locations other than the neck region, which in some circumstances can lead to a double-neck structure; when the two constrictions are well separated from each other, the total resistance is that due to two constrictions in series resulting in conductance values which may take fractional values of  $g_0$ . Additionally, for sufficiently thin wires successive narrowings are localized at the narrowest neck (typically for wire diameters less than  $\sim 20$  Å, depending on the ratio of the neck radius to the global axial radius of curvature of the wire), while for thicker ones, i.e., at the earlier stages of pulling, narrowings may occur occasionally at thicker regions, leaving the area and shape of the narrowest constriction essentially unaltered. Since the conductance of the wire is determined mainly by the dimensions and shape of the narrowest constriction (i.e., the number of conducting channels is given by the number of transverse electronic states at this region), such occurrences can lead to the development of extended plateaus in the conductance measured versus the extent of elongation [1(c)].

It should also be remarked that the force per unit area in the neck region of the wire, obtained from the simulated force or stress records, displays the same general behavior as the overall force [Fig. 3(a)] and exhibits critical uniaxial stress values of 5 to 6 GPa, which, when resolved along the glide directions, yield critical resolved shear stress values of  $\sim 4$  GPa. This value, which is over an order of magnitude larger than that of bulk gold [17], is in approximate agreement with the average value of  $J_2$  for the neck region [Fig. 3(b)] and is comparable to the theoretical value for Au (1.5 GPa) in the absence of dislocations [17], as well as being close to our earlier theoretical predictions [2(a)] which were confirmed by experiments [5(c),18]. The mechanical “ideal” nature of the nanowires, which can be related to their characteristic small dimensions and the inability to support dislocation sources (e.g., Frank-Read sources [19]), are correlated with the observed reversibility of their properties [20]. We remark here that similar stress accumulation and relief mechanisms and atomic structural rearrangement processes, including multiple glide, occur during both extension and compression of the wire [see Figs. 3(a)

and 3(b) and 4(b) and 4(b')]; it should be noted that while we observe overall mechanical and structural reversibility, certain variations in atomic positions occur for equivalent (in length) configurations of the nanowire [compare Figs. 4(a) and 4(c')].

The calculated [16] conductance [Fig. 3(c)] portrays the structural variations in the nanowire, and each of the step rises correlates directly with the signatures of the structural transformations [compare Fig. 3(c) with 3(a) and 3(b)]. Furthermore, the variation of the uniaxial strain during the stress accumulation intervals (between yield, i.e., transformation, stages) is accompanied by continuous contractions and expansions of the wire's cross-sectional areas for the elongation and compression cycles, respectively. This is reflected in the slopes of the conductance plateaus, in both the calculations [Fig. 3(c)] and the experimental (Fig. 1) results.

The direct correlation between the measurements and the atomistic mechanisms obtained via MD simulations provides significant insights pertaining to the mechanical response and electrical transport properties of nanowires. The demonstrated ability to reversibly manipulate these properties at room temperature using common instrumentation opens exciting avenues for further investigations and potential applications, such as switching [13,21]; of course, to make such applications practical, issues pertaining to operational speed, stability, lifetime, and control of individual junctions must be addressed.

Technical conversations with Professor W. deHeer are gratefully acknowledged. This research is supported by the U.S. Department of Energy and the AFOSR. Simulations were performed on Cray computers at the National Energy Research Supercomputer Center, Livermore, California, and the GIT Center for Computational Materials Science.

- 
- [1] (a) E.P. Bowden and D. Tabor, *Friction* (Anchor Press/Doubleday, Garden City, NY, 1973); (b) For a recent review see B. Bushan, J.N. Israelachvili, and U. Landman, *Nature* (London) **374**, 607 (1995); (c) U. Landman, J. Gao, and W.D. Luedtke, *Langmuir* (to be published).
- [2] (a) U. Landman, W.D. Luedtke, N.A. Burnham, and R.J. Colton, *Science* **248**, 454 (1990); (b) U. Landman and W.D. Luedtke, *J. Vac. Sci. Technol. B* **9**, 414 (1991).
- [3] J.I. Pascual, J. Mendez, J. Gomez-Herrero, A.M. Baro, N. Garcia, and Vu Thien Binh, *Phys. Rev. Lett.* **71**, 1852 (1993).
- [4] J.I. Pascual, J. Mendez, J. Gomez-Herrero, A.M. Baro, N. Garcia, U. Landman, W.D. Luedtke, E.N. Bogachek, and H.-P. Cheng, *Science* **267**, 1793 (1995); *J. Vac. Sci. Technol. B* **13**, 1280 (1995).
- [5] (a) N. Agrait, J.G. Rodrigo, and S. Vieira, *Phys. Rev. B* **47**, 12345 (1993); (b) N. Agrait, J.G. Rodrigo, C. Cirvent, and S. Vieira, *Phys. Rev. B* **48**, 8499 (1993);

- (c) N. Agrait, G. Rubio, and S. Vieira, *Phys. Rev. Lett.* **74**, 3995 (1995).
- [6] L. Olesen, E. Laegsgaard, I. Stensgaard, F. Besenbacher, J. Schiøtz, P. Stoltze, K.W. Jacobsen, and J.N. Nørskov, *Phys. Rev. Lett.* **72**, 2251 (1994).
- [7] L. Kuipers and J.W.M. Frenken, *Phys. Rev. Lett.* **70**, 3907 (1993).
- [8] A. Stalder and U. Durig, *Appl. Phys. Lett.* **68**, 637 (1996).
- [9] J.M. Krans, J.M. van Ruitenbeek, V.V. Fisun, I.K. Yanson, and L.J. de Jongh, *Nature* (London) **375**, 767 (1995), and references therein.
- [10] J.L. Costa-Kramer, N. Garcia, P. Garcia-Mochales, and P.A. Serena, *Surf. Sci.* **342**, L1144 (1995).
- [11] E.N. Bogachek, A.M. Zagoskin, and I.O. Kulik, *Fiz. Nizk. Temp.* **16**, 1404 (1990) [*Sov. J. Low Temp. Phys.* **16**, 796 (1990)].
- [12] A.G. Scherbakov, E.N. Bogachek, and U. Landman, *Phys. Rev. B* **53**, 4054 (1996).
- [13] E.N. Bogachek, A.G. Scherbakov, and U. Landman, *Phys. Rev. B* **53**, 13 246R (1996).
- [14] The parametrization used is after J.B. Adams, S.M. Foiles, and W.G. Wolfer, *J. Mater. Res.* **4**, 102 (1989).
- [15] G. Dieter, *Mechanical Metallurgy* (McGraw-Hill, New York, 1967); see also U. Landman, W.D. Luedtke, and E.M. Ringer, in *Fundamental of Friction*, edited by J.L. Singer and H.M. Pollock (Kluwer, Dordrecht, 1991), p. 463.
- [16] V.I. Fal'ko and G.B. Lesovik, *Solid State Commun.* **84**, 835 (1992); J.A. Torres, J.I. Pascual, and J.J. Saenz, *Phys. Rev. B* **49**, 16581 (1994). The calculation of the conductance uses a modified Sharvin expression which is based on Weyl's theorem [see, e.g., P.M. Morse and H. Feshbach, *Methods of Theoretical Physics* (McGraw-Hill, New York, 1953), p. 761], relating the number of transverse states (channels) in the narrowest part of the junction to the cross-sectional area and the circumference of the narrowing. These quantities were estimated from the geometries of atomic wire configurations obtained during the simulation (see, e.g., selected cross-sectional configurations in Fig. 4). Because of strong screening in metals the effective potential confining the electrons in the wire is short ranged [as also found in recent local density functional calculations of metallic wires by U. Landman, R.N. Barnett, and W.D. Luedtke, *Z. Phys. D* (to be published)] approximating well a hard-wall boundary potential, corresponding to the Dirichlet boundary condition used in derivation of the Weyl theorem.
- [17] A. Kelly and N.H. MacMillan, *Strong Solids* (Clarendon, Oxford, 1986).
- [18] After submittal of our manuscript, apparent pressures in the range of 3 to 6 GPa measured for Au nanowires at 300 K, in agreement with our earlier [2(a)] and current predictions, have been reported; see G. Rubio, N. Agrait, and S. Vieira, *Phys. Rev. Lett.* **76**, 2302 (1996).
- [19] D. Hall, *Introduction to Dislocations* (Pergamon, Oxford, 1975).
- [20] C. Herring and J.K. Galt, *Phys. Rev.* **85**, 1060 (1952).
- [21] D.P.E. Smith, *Science* **269**, 371 (1995).